Published as https://doi.org/10.1021/acscatal.1c05739

The Dynamic Role of Gold d-orbitals during CO oxidation in aerobic conditions

Alessandro Longo[1,2*], Francesco Giannici[3], Maria Pia Casaletto[2*], Mauro Rovezzi[1,4], Christoph Sahle[1], Pieter Glatzel[1], Yves Joly[5], Antonino Martorana[3].

[1] ESRF - The European Synchrotron, CS 40220, 38043 Grenoble Cedex 9, (France).
[2] Istituto per lo Studio dei Materiali Nanostrutturati, Consiglio Nazionale delle Ricerche, Via Ugo La Malfa 153, 90146 Palermo, (Italy).
[3] Dipartimento di Fisica e Chimica, Università di Palermo, Viale delle Scienze, I - 90128 Palermo, (Italy).
[4] Universitè Grenoble Alpes, CNRS, IRD, Irstea, Météo France, OSUG, FAME, 71 Avenue des Martyrs, CS 40220, 38043, Grenoble (France).
[5] Universitè Grenoble Alpes Inst NEEL, 38042 Grenoble (France) and CNRS, Inst NEEL, 38042 Grenoble (France).

Abstract

CO oxidation at room temperature was performed in aerobic and anaerobic conditions, and High Energy Resolution Fluorescence Detection X-ray Absorption Spectroscopy (HERFD-XANES) at Au L3 edge was used to study gold catalysts supported on ceria in order to unravel the role of gold 5d orbital modifications occurring during the activation of molecular oxygen. The

variations in the HERFD-XANES resonance peak, directly correlated with d-band occupancy, were monitored *in situ* during the redox process. An interesting oscillating behavior during the oxygen treatments was observed and it can be related to a corresponding oscillation in the population of gold d-orbitals during the oxidation of CO. The interpretation of X-ray spectroscopy data is supported by *ab initio* simulations performed using the FDMNES code.

Keywords: In situ, HERFD, XANES, d-bands, CO oxidation, Au/CeO_2.

Corresponding Authors

* *Alessandro Longo, alessandro.longo@esrf.fr*

* *Maria Pia Casaletto, mariapia.casaletto@cnr.it*

Introduction

CO oxidation on supported gold nanocatalysts has been a paradigmatic and pivotal problem in catalysis in the last three decades [1-11] and recent literature confirms that it still remains an intriguing argument [12-16]. The apparently simple reaction is difficult to understand because many factors, such as the size of gold particle, the valence state of gold and gold interaction with the support, would dramatically influence the catalysts activity. Normally all these factors occur together, and disentangling their effects is difficult [7, 8, 10, 11]. This issue stimulated a long-standing scientific debate on the nature of the gold active site, resulting in a virtuous synergy between theoretical and experimental works [13,17,18,19]. However, model catalyst systems with controlled gold oxidation states are difficult to obtain, and the identification of the real active site for the CO oxidation is still a compelling subject, perfectly suited for a direct experimental study of the reaction mechanism under working conditions.

The details in the occupancy of the *d*-band of the supported metal catalyst are pivotal for describing the origin of catalytic activity [19-22]. The CO oxidation reaction gold catalyzed is usually interpreted explained according to the so-called *d*-band model, in which substrate-adsorbate bonds are formed. The strength of the new bonds depends on the position of the *d*-band center such that a d-band closer to the Fermi level will result in stronger interaction. The *d*-band center of bulk gold is located far below of the Fermi level [19]. However, as the size of gold clusters decreases below 5 nm, a significant perturbation of Au electronic structure occurs. Upon nanoscaling, it has been shown that gold *d*-band center shifts to energies closer to the Fermi level. This affects the formed antibonding orbital originated by the interaction of the molecule with the metal, which will have its energy shifted above the Fermi energy level. Thus, the *d*-band center of gold reduces its occupancy resulting less filled [19, 22]. Additionally to the the *d*-band shifts, the very high

dispersion of nanosized gold clusters lowers the number of hybridized valence states: this in turn makes the d-band states distribution sharper and more defined [13], with less significant splitting from spin-orbit coupling [19, 23].

In any case, the gold cluster size is not the only contributing factor to be considered. The support oxide also directly influences the electronic structure of the deposited gold clusters by different mechanisms, e.g. strain-induction and charge transfer [15]. In this respect, a key structural argument used to explain the high activity of metal oxide supported gold clusters is based on the idea of peripheral sites formed at the junction between the gold cluster and the substrate [11,15]. These peripheral atoms are supposed to show high activity towards adsorption, due to the higher coordinative unsaturation in comparison with the bulk ones, and to be the preferred sites where the reaction takes place. However, the evidences on gold-catalyzed CO oxidation are still not fully conclusive, and at times even contradictory.

For instance, it was reported that gold octamers (Au8) bound to oxygen-vacancy F-center defects on Mg(001) are the smallest clusters capable of catalyzing the low-temperature oxidation of CO to CO_2, while clusters deposited on undefective surfaces remain chemically inert. The charging of the supported clusters plays a key role in promoting their chemical activity [18]. Guo et al. showed that the metallic gold component in clusters are much more important as active sites than Au^+ species for the CO oxidation [14, 16]. Moreover, against the general speculation that the active sites are immobile, it has been shown that Au clusters are not rigid in operating conditions. While large Au nanoparticles effectively remain rigid, very small Au clusters lose their internal structures and become almost disordered, inducing considerable sizable rearrangements and resulting in the formation of cyclically "uncoordinated" atoms on the surface [18]. On the other side, other authors claimed that the single gold atoms dispersed in a reducible defective support

are the real active species [24, 25]. Irrespective of all the possible structural scenarios, which are not able to fully explain the electronic modification occurring in the metal particles, it is commonly accepted that the charge transfer, originating by metal-support interaction, induces a local perturbation in the electronic structure of the gold clusters. Such a perturbation is mostly located around the cluster itself, or at detached atom sites, and depends strongly on catalyst pre-treatments that may influence the electronic state of gold species ($Au^{\delta+}$, Au^0, $Au^{\delta-}$) [26]. The changing of the metal electronic state allows the π* antibonding orbital of oxygen to interact with the metal *d*-band. As the antibonding orbital occupancy rises, the O=O bond is weakened and stretched, and it's therefore activated to react with CO [11, 20, 22, 27]. Interestingly, the mechanism by which molecular oxygen is activated indicates the (transient) formation of gold-oxygen complexes, which activate O_2 on the gold particles [16, 20, 28]. Notably, the activation is detected as an increase of the Au L_3 XANES resonance peak, which indicates the corresponding gold *d*-band occupancy. However, important questions concerning the reversibility of the gold-oxygen complex formation, its evolutions, and the possible restoration of metal-support interaction during the oxidation process are still unsolved.

In recent literature, conventional X-ray absorption spectroscopies, which are able to solve the gold local environment in different chemical conditions, are still the main characterization techniques [16, 20-22, 26-29]. The XAFS signal, as it happens for bulk analytical techniques, arises from the combination of all gold atoms. Unfortunately, due to the low resolution achievable in a conventional XAFS experiment, the variations in the d-band occupancy (i.e. the XANES region) are hard to be highlighted and interpreted. The high-energy-resolution fluorescence detection (HERFD) technique can then be used to overcome limitations of conventional XAFS techniques, acquiring the intensity of a single fluorescence line corresponding to a

specific excited state decay, using a narrow energy resolution. *In situ* application of HERFD XAFS to several catalytic systems has recently given fundamental insights in structure-properties relationships [30, 31].

In this work, we prepared gold catalysts supported on ceria through the deposition/precipitation method, and performed in situ HERFD-XANES during the CO oxidation reaction performed both in anaerobic and aerobic conditions. Ex-situ XRD and XPS characterization provided information on the geometrical structure and surface chemical composition of the catalysts. The variations in the HERFD-XANES showed an clear oscillating behavior during the oxygen treatments which have been related to a corresponding oscillation in the population of gold d-orbitals during the oxidation reaction. Moreover, in aerobic condition, the d-band reaches an intermediate state which corroborates the dynamic role of the gold clusters during the catalysis.

Modeling of the Au L3 edge features were performed by ab initio simulations using the Finite Difference Method Near Edge Structure (FDMNES) code [32].

Experimental Section

Catalyst Preparation

Au/CeO_2 powders, with an Au loading of 1.0 and 3.0 % w/w (determined by ICP-AES), were prepared by homogeneous deposition/precipitation method, using urea as precipitating agent [33, 34]. Hereafter, the resulting catalyst is labelled as “fresh sample”. A reference gold catalyst supported on carbon substrate (Au/C sample) was purchased from Premier Chemicals Limited, UK (NanAucat™ Gold Oxidation Catalyst).

X-ray diffraction (XRD)

XRD measurements were carried out with a Bruker D5000 equipped with a

Cu anode (Kα radiation λ=1.5418 Å) and a graphite monochromator. A proportional counter and a 0.05° step size in 2θ were used. The assignment of the crystalline phases was based on the JPDS database. As evident in the XRD patterns of the Au ceria supported catalysts, showed in fgure S1, any metal particles were detected. In agreement with previous work, this suggested an average custers size below the 4 nm.[29, 33, 34] For the Au/C sample the average particle size of gold clusters was calculated using the Scherrer equation, indicating 2.8-3.5 nm cluster size.

X-ray photoelectron spectroscopy (XPS)

XPS analysis were performed by a VG Microtech ESCA 3000 Multilab spectrometer with Al Kα source ($h\nu$= 1486.6 eV). The binding energy scale (BE) was charge compensated by using C 1s peak (BE = 285.1 eV) from adventitious carbon. Curve fitting was performed with Voigt peak shape after Shirley background subtraction according to Sherwood [35]. Relative concentrations of chemical elements were calculated by a standard quantification routine, including Wagner's energy dependence of attenuation length [36] and a standard set of VG Escalab sensitivity factors. The uncertainty on the atomic quantitative analysis is about ± 10%. Assignment of photoelectron signals and peak components was determined according to literature reference database [37]. The results of the analysis are reported in figure S3 iin the ESI file.

In situ HERFD-XAFS

X-ray absorption spectroscopy measurements were carried out at the high-brilliance XAFS-XES beamline ID26 and at the Inelastic Scattering beamline ID20 of the European Synchrotron Radiation Facility (ESRF) in Grenoble, France [38, 39]. *In situ* and *ex situ* HERFD-XAFS measurements were performed at room temperature using the "microtomo reactor" available at ESRF.

The gas atmosphere in the reactor was controlled by three mass-flow controllers (Bronkhorst). The catalyst was exposed to different atmospheres as follows: pure He, 1% CO in He, and 20% O_2 in He (Air Liquide). The reactor exhaust was connected to a mass spectrometer (Pfeiffer QMS200), which mainly was used for monitoring the CO2 formation during the HERFD-XANES evolution (see figure S3 in ESI file).

All X-ray spectroscopic measurements were performed *in situ* under constant flux (20 mL min^{-1}) of gas through the reactor.

Each treatment cycle consisted of an exposure to CO and O_2 in succession, for 50 min and 30 min, respectively. Before each gas switch, the reactor was purged for 5 min with helium.

In order to avoid radiation damage, HERFD-XANES spectra were acquired every 10 s between 11900 and 12080 eV, with a continuous energy scan and in 200-380 different spots of the pelletized powder sample. For each measurement, different points of the pellet were scanned and then all the scans were summed up. For the *in situ* measurements, the spectra were recorded with the same energy steps and energy interval every 15s. In this case, 180 different spots were scanned on the sample in order to follow the structural kinetic for one hour. Full HERFD-EXAFS spectra, collected as the static XANES but over a 600 eV range, were also measured under steady-state conditions and used to normalize the intensity of the HERFD-XANES data.

HERFD-EXAFS data analysis

HERFD-EXAFS spectra (two scans per sample) were energy-calibrated, averaged and further analyzed using GNXAS [40]. In this approach, the local atomic arrangement around the absorbing atom is decomposed into model atomic configurations containing 2, ..., *n* atoms. The theoretical EXAFS signal $c(k)$ is given by the sum of the *n*-body contributions γ^2, γ^3, ..., γ^n that take into

account all the possible single and multiple scattering (MS) paths between the n atoms. The modeling of $\chi(k)$ to the experimental EXAFS signal allows to refine the relevant structural parameters of the different coordination shells (see figure S4 and S5 in the ESI file). The quality of the model is also checked by comparison of the experimental EXAFS signal Fourier transform (FT) with the FT of the calculated $\chi(k)$ function. The coordination numbers and the global fit parameters that were allowed to vary during the fitting procedure were the following: the distance R(Å), Debye-Waller factor (σ^2) and the angles of the γ^n contributions. The edge energy E_0 was fixed at 11919 eV.

HERFD-XANES data analysis

HERFD-XANES spectra at the Au L3 edge were modeled using the Finite Difference Method Near Edge Structure (FDMNES) software [41, 42]. The simulations were performed by using the multiple scattering theory based on the muffin-tin (MT) approximation for the potential shape of the Green scheme. The MT radii were tuned to have a good overlap between the different spherical potentials. A relativistic spin-orbit calculation was performed and the Hedin-Lundqvist exchange potential was applied. The approximation of excited absorbing atoms was used, which, in this case, better reproduced the experimental data [41]. In order to model the variations in the average electronic occupancy on the metal particles during the reaction, the semi-empirical parameter *screening* was used. [42] In this respect, a set of Au L3 edge spectra, corresponding to different values of *screening* were calculated. Then, the calculated spectrum was matched to the experimental data set for best agreement. This scheme of calculation was repeated for different clusters radii from 6 to 10 Å (see Figure XANES in ESI).

Results and discussion

1. Au XANES features

The XANES region of the X-ray absorption spectrum provides information about the density of states above the Fermi level. In Figure 1 the static HERFD-XANES spectra of 3% Au catalysts, together with those of different gold references, are comparatively shown. In Panel **I** three main features: **a, b** and **c** of the experimental spectrum are highlighted. In particular, peak **a** is commonly known as the "white line", and it is due to $2p_{3/2} \rightarrow 5d_{5/2,3/2}$ transitions [20, 22, 23, 28, 29, 43, 44]. For metals with vacant *d*-orbitals this resonance is a sharp peak, and its intensity reflects the density of the unoccupied *d* states. This explains the very sharp white line in the gold(III) reference spectrum compared to the other spectra (see inset Figure 1), due to empty 5d states,. The white line is in contrast quite suppressed both in the gold foil and in Au/C, as evidenced in Figure 1. On the other hand, a small peak is clearly visible in Au/CeO_2.

In the case of Au metal clusters, the 5*d* band is nominally full and, therefore, no resonance peak is expected. However, hybridization of the 5*d* orbitals with the overlapping 6s and 6p orbitals determines an overall charge redistribution resulting in a small amount of 5*d* holes above the Fermi level [45, 46]. Moreover, the charge distribution and the relative occupancy, which is affected by the cluster size, can be affected by ligand binding and by interactions with the support [43-45]. Then, even in the absence of ionic gold, the presence of a resonance peak is an evidence for such an electronic perturbation, which increases the 5d-hole populations [45, 46]. It is important to notice the resonance peak cannot be modeled as the sum of ionic (either Au^{3+} or Au^{+}) and Au^{0} components. In fact, fitting of the spectra using component analysis finds Au cations at about 8-10% or 30-40%, depending on the cationic reference spectrum (Au^{3+} or Au^{+}) used in the analysis. This is in spark contrast with the reported XPS results (see below), where the ionic contribution cannot exceed 3% overall. In addition, such a component

analysis can only be applied to a very limited energy range of the spectrum, in which the peak is present, lacking robustness.

The Au 4f XPS analysis shows a single Au $4f_{7/2}$ peak assigned to Au^0 in 3% Au/CeO_2 [35, 37, 45], with no evidence of oxidized gold species. For the 1% Au/CeO_2 a secondary small component is attributed to Au^+ [35, 37, 47], corresponding to about 25% of total peak area.

It can be inferred that the increased resonance peak mainly brings a contribution accountable to the metal support interaction [29, 44-46].

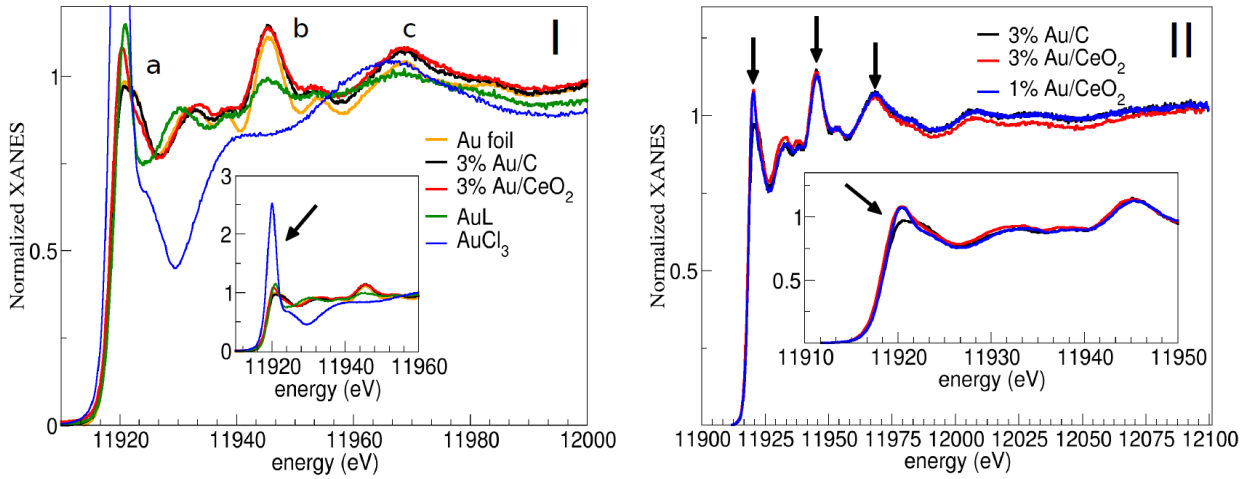

Figure 1. Panel I: XANES spectra of 3% Au/C (black), 3% Au/CeO2 (red), Au foil (orange), gold(I) (dark green) [$(C_2H_5)_3PAuCl$] and $AuCl_3$ (blue). The main peaks are labeled as a, b and c. In the inset, the whole intensity of the Au^{3+} white line is compared to others. Panel II: Comparison of 3% Au/CeO_2 (red) with 1% Au/CeO_2 (blue) and Au/C sample (black). The arrows highlight the strong similarities between 1% and 3% Au/CeO_2.

The two peaks labeled **b** and **c** in Figure 1 give information about the gold atomic arrangement. Remarkably, these peaks are diagnostic for the fcc atomic arrangement with more than two coordination shells and they are connected to the lattice parameter and the size of the metal gold clusters [43,44]. As the cluster size decreases, a shift towards higher energies and a broadening of the peaks occurs. Since peaks **b** and **c** are very similar in all the supported samples, it can be argued that, irrespective to the different

support used, the gold catalysts have comparable metal clusters dimension (see Figure 1, Panel II).

2. In situ HERFD-XANES

In situ measurements were performed to follow the Au electronic state variations occurring during a redox cycle at 298 K, monitoring the resonance peak relative to 2p → 5d transition (peak **a**).

Results of the *in situ* measurements collected during the reducing treatment in CO are reported in Figure 2. After switching from inert gas to CO, an induction time (about 10 min) is observed before reduction. Upon reduction, an abrupt decrease of the resonance peak occurs, about 10% of the normalized peak intensity.

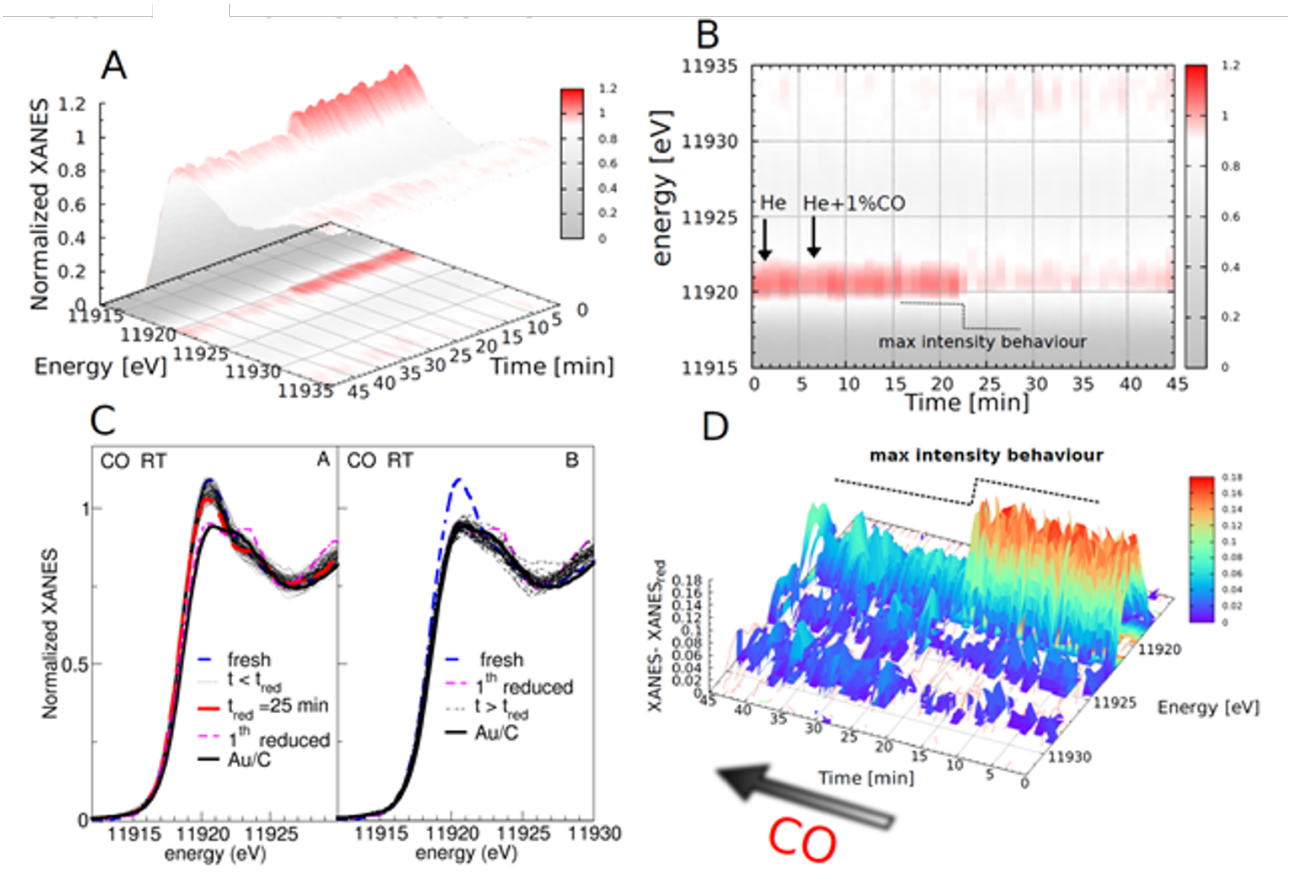

Figure 2. Panel A: Evolution of HERFD-XANES spectra of 3% Au/CeO_2 catalyst during the CO treatment. Panel B: 2D projected intensity map

(time/energy) relative to panel A. Panel C: Superimposed XANES spectra, of Au/CeO2 and Au/C during the CO reduction. For sake of clarity the kinetic has been divided before and after the time t_{red} (indicated by the red line in the panel) indicatind the beginning of the reduction. Panel D: Relative intensity of the peak maximum minus the averaged reduced spectrum.

The reduction of the peak intensity is expected. CO reduces the ceria support inducing a strong modification of the oxide surface on which gold resides [48]. Ultimately, the metal-support interaction, arising from metal clusters with the surface oxygen bound with the support, is completely inhibited. The 5*d* band of gold is filled and then a decrease of the resonance peak is observed. No variation of the resonance peak was detected when the same reaction performed on the Au catalyst deposited on carbon, as shown in Figure 3.

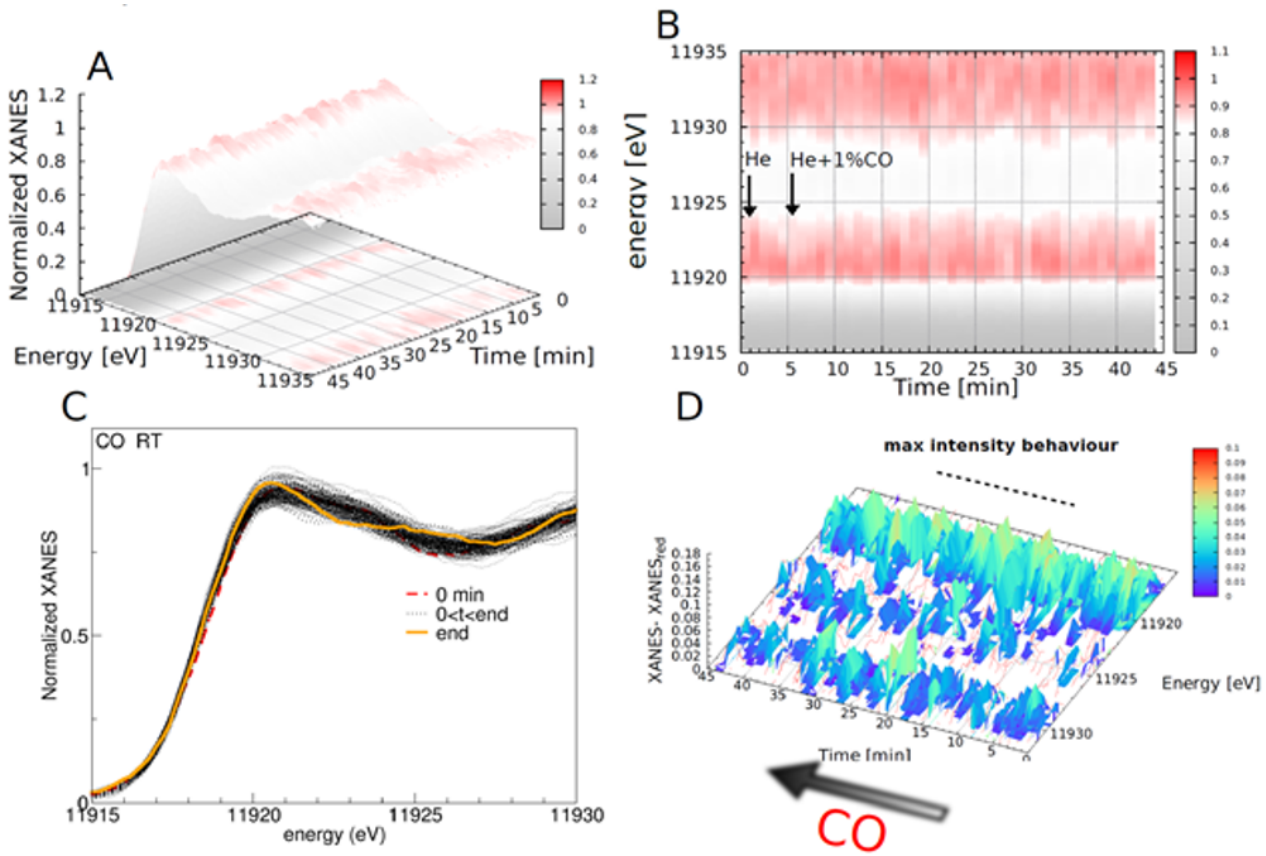

Figure 3. Panel A: Evolution of HERFD-XANES spectra of 3% Au/C catalyst during the CO treatment. Panel B: 2D projected intensity map (time/energy) relative to panel A. Panel C: XANES spectra. Panel D: Relative intensity of the peak maximum minus the averaged reduced spectrum.

Figure 4 shows a full redox cycle carried out immediately after the exposure of the CO. After 5 min of oxygen treatment, an increase of the XANES resonance peak is detected. Then, an oscillating behavior begins, resulting in an increase and decrease of the peak intensity during the whole oxidation process, as evidenced in Panels B and C of Figure 4. After switching to CO, a sharp lowering of the resonance peak was again observed.

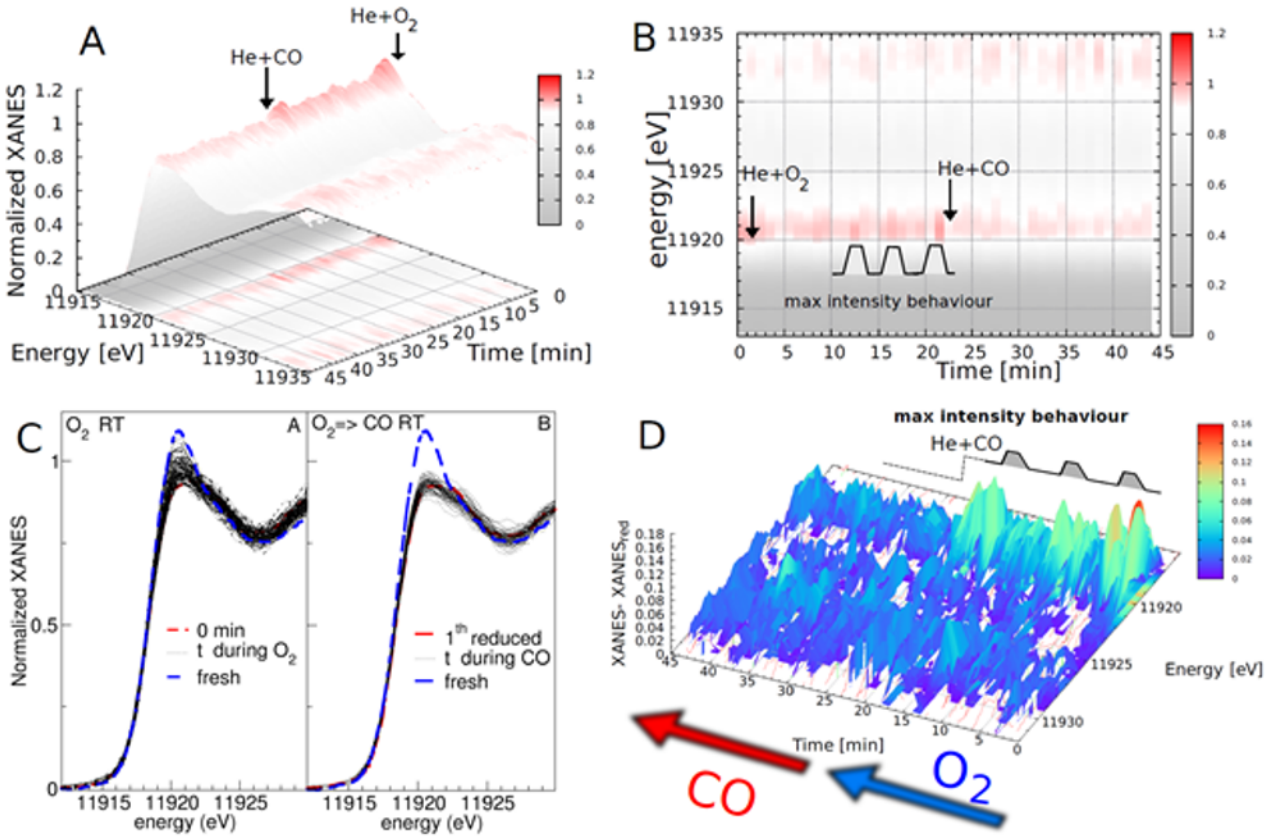

Figure 4. Panel A: Evolution of HERFD-XANES spectra of 3% Au/CeO_2 during the O_2/CO redox cycle. Panel B: 2D projected intensity map (time/energy) relative to panel A. Panel C: XANES spectra. For sake of clarity the kinetic has been divided before and after the time t_{red} (indicated by the red line in the panel) in which the reduction starts.Panel D: Relative intensity of the peak maximum minus the averaged reduced spectrum.

The difference obtained in the two subsequent experiments is conclusive to distinguish a different *d*-band occupancy in reduced and oxidized state.

A similar trend was observed also for 1% Au/CeO_2, as summarized in Figure 5. In these plots, average d-band occupancy is probed through peak intensity,

and three different values can be singled out and correlated to different redox condition: fresh, reduced and oxidized. The comparison evidences that the peak intensity decrease is delayed by 20 min and the oscillating behavior is less evident in 1% Au/CeO_2. All considered, the average *d*-band occupancy is similar to that obtained for 3% Au/CeO_2, as shown in Figure 5.

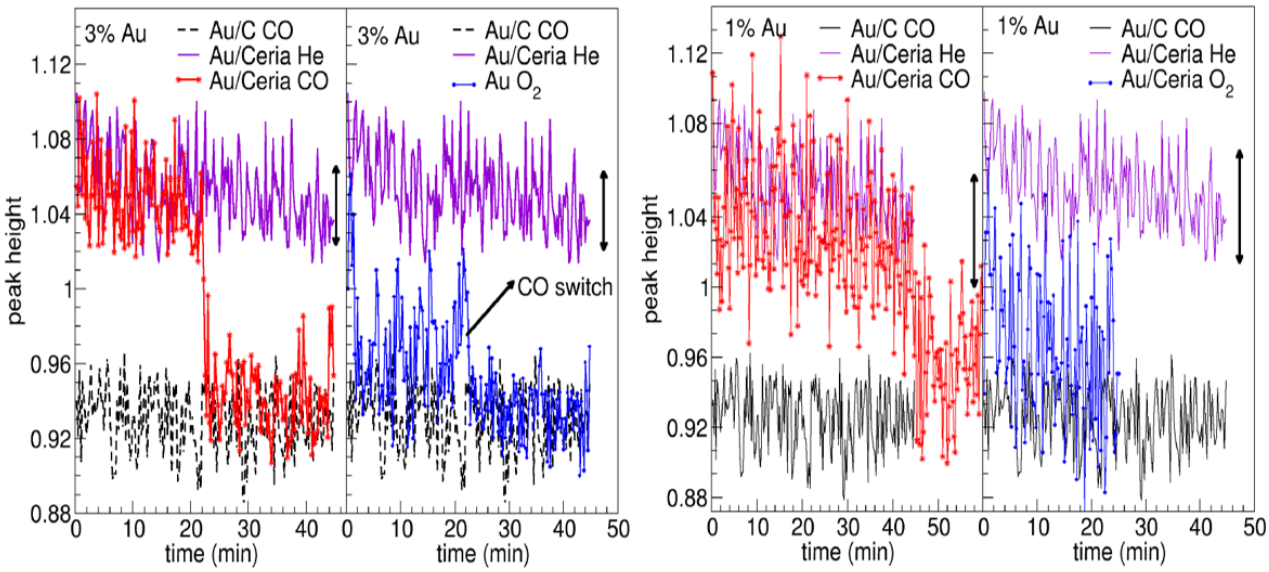

Figure 5. Time-resolved peak intensity for 3% Au/CeO2 (left panel) and 1% Au/CeO2 (right panel) for the redox treatments in constant flux (20 mL min^{-1}) of gas (He/CO or He/O_2) The arrows indicate the fluctuation of the maximum value of the white line (approx. ±0.02 and ±0.03, respectively). Au/C is shown for comparison.

A further fresh 3% Au/CeO_2 sample was exposed to a CO/O_2 mixture (Figure 6), and a continuous decrease of the resonance peak was observed. Interestingly, after 25 min, the resonance peak reached a constant trend, whose average value matches the one obtained in the re-oxidation reaction of the reduced sample. This value lies between those obtained for the fresh and the fully reduced catalyst. This result, compared with those achieved in the other cycles, is summarized in Figure 7.

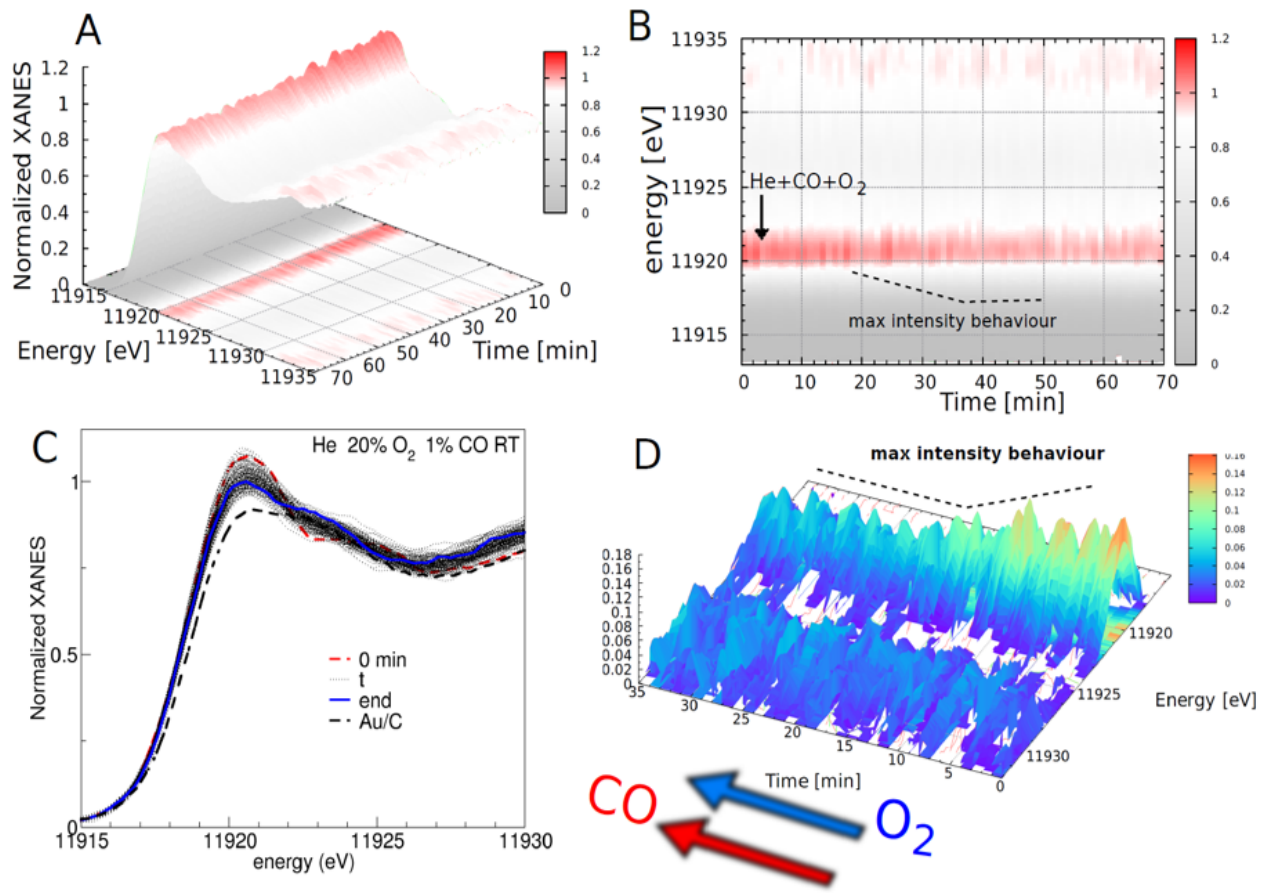

Figure 6. Panel A: Evolution of HERFD-XANES spectra of 3% Au/CeO_2 during the O_2+CO mixture treatment. Panel B: 2D projected intensity map (time/energy) relative to panel A. Panel C: XANES spectra. Panel D: Relative intensity of the peak maximum minus the averaged reduced spectrum.

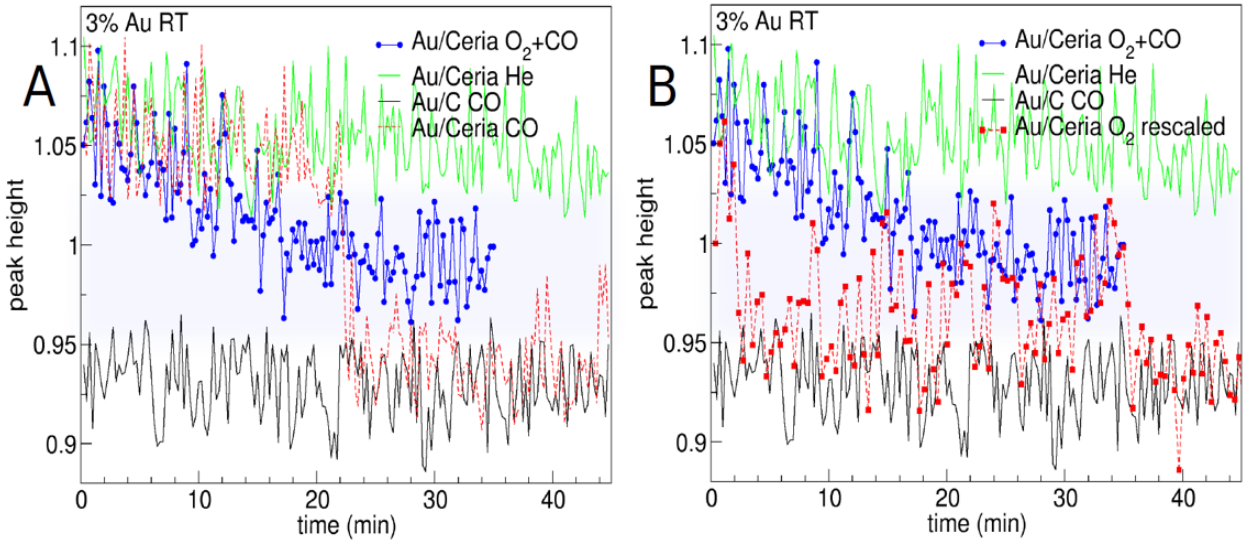

Figure 7. Time-resolved peak intensity of 3% Au/CeO_2 during different treatments. Panel A: Comparison of the CO+O_2 mixture with respect to CO reduction. Panel B: Comparison of the CO+O_2 gas mixture with respect to O_2

oxidation. The results measured in O_2 were time-shifted for better comparison. Results of Au/C reduction in CO are reported as a reference.

3. XANES modeling and discussion

As expected, the CO oxidation reaction mechanism is different in the aerobic and anaerobic condition. In anaerobic conditions, and abrupt change of *d*-band occupancies correlated with the sudden change of the resonance peak is observed after an induction period. CO conversion starts as soon as the CO/He mixture reaches the catalyst, as witnessed by the mass quadrupole signal out of the reactor. The CO oxidation involves the consumption of oxygen atoms, either adsorbed or in the lattice. The latter process leads to the reduction of surface or subsurface Ce(IV) species, and it does not result in any modification of the metal gold clusters [48, 16, 22]. After the oxygen depletion of the support surface layer, bulk reduction takes place, and the metal clusters are fully reduced losing their interaction with the support as well [47]. So during the CO oxidation reaction in anaerobic condition, most oxygen atoms are provided by the ceria support, which, will be strongly defective at the end. When the re-oxidation of the sample starts, molecular oxygen is first bound on the metal cluster surface. Therefore, the 5*d* band occupancy decreases, and a corresponding increase of the resonance peak is detected. In this step, molecular oxygen is activated and it can be conveyed to the ceria lattice in order to refill the O^{2-} vacancies in the support [49]. The transfer of activated oxygen to the oxide, breaking the Au-O bond, corresponds to an increase of the gold 5*d* band occupancy, with the consequent lowering of the resonance peak (see Figure 4). It can be argued that, during the oxygen migration in the ceria lattice, an induction is needed before the metal can adsorb O_2 again. During this time, the gold cluster keeps the 5*d* band full, so no relevant change of the resonance peak is observed.

The acquisition time used for the *in situ* measurements (10 s) is definitely slower than the turnover of oxygen reduction. Therefore, the time averaging of the sample in different d-band occupancies could explain the irregular oscillating behavior.

A different scenario occurs when CO oxidation takes place in the presence of oxygen (aerobic conditions). In this case, molecular oxygen adsorbed on the metal surface, or in contact with the Au cluster, is activated and reacts directly with CO [49]. Due to the simultaneous process of emptying and filling the Au 5*d* band, an average occupancy value is reached, which results in a smooth variation of the resonance peak. The gradual decrease of the white line lasts around 15 min before reaching the eventual average value (see Figure 7): therefore, an initial structural rearrangement of the metal clusters and the formation of active gold-oxides species must be taken into account [13,15-16, 22, 28, 49-51].

In order to validate the hypothesis that the variation of resonance peak upon the different chemical treatments can be ascribed mainly by the variation of the d-band occupancy, the XANES spectra were simulated from first principles with the FDMNES package (Figure 8).

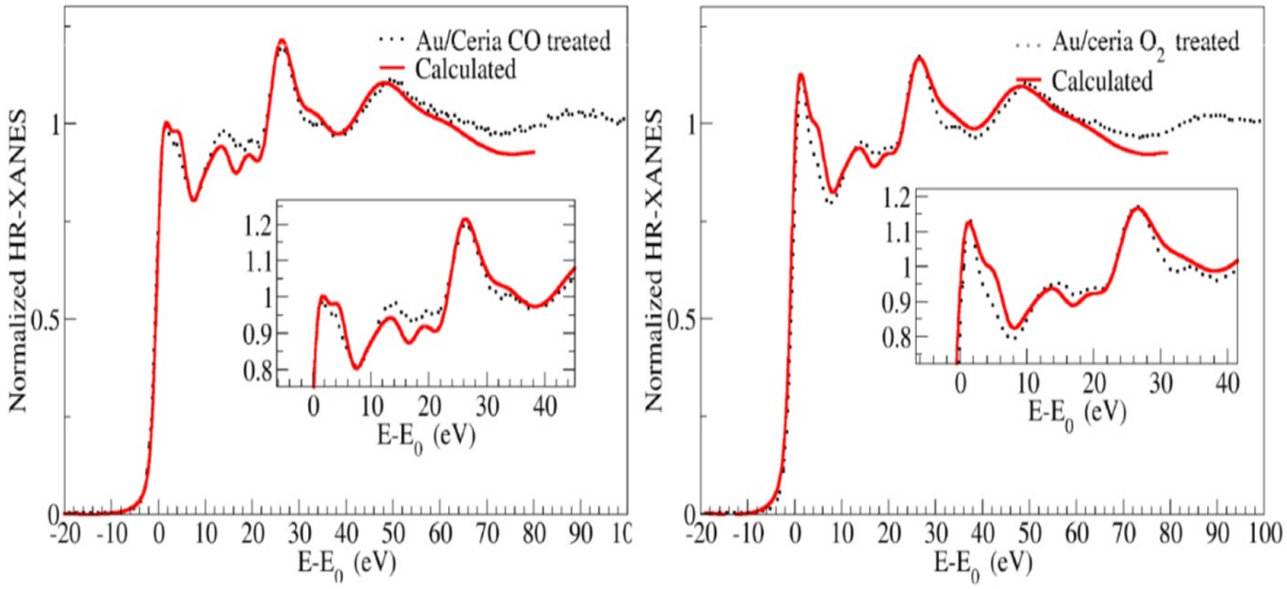

Figure 8. HERFD-XANES spectra and simulations of 3% Au/CeO_2. Panel A:

Observed spectrum reduced in CO (black), and model (red). Panel B: Observed spectrum re-oxidized in O_2 (black), and model (red)

The key parameter to reproduce the variable 5d band occupancy is the semi-empirical correction term *screening*. By changing the screening parameter, the electronic charge in the non-full valence orbital of the absorber is modified by placing an additional electron in the first non-occupied state, while the absorbing atom remains (almost) neutral [52, 53].

Within the energy range of interest, all main features of the electronic band structure around the Au L3 edge are reasonably well reproduced by applying *screening* values of 0.9 for reduced catalyst. For the fresh and re-oxidized *screening* was kept at the default value of one, representing the fully removed core electron. The fact that the positive core-hole charge is not fully screened (only 0.1 charge missing in the unoccupied level) suggests to a correlation effect caused by the presence of the excited 5*d* electron hindering the screening process [52] which corroborates the possible interaction of the metal cluster either with the ceria support or the adsorbed oxygen molecules. The fact that *screening* value is not needed for the reduced sample, reflects a more filled 5*d* orbital, which is connected in turn to a Fermi energy that shifts upward, with respect to the fresh or oxidized samples. Notably, the metal cluster radius considered in the model is 9 Å, which is the best size to reproduce the peaks centered around 28 and 49 eV after the main edge. The cluster size is in good agreement with the average coordination numbers obtained in the EXAFS analysis reported in ESI. In addition, no cationic species were considered in the calculation showed in Figure 8.

The increase of the resonance peak in gold ceria catalyst after exposure to oxygen is not fully surprising and it has been already reported in the literature [16, 22, 26]. However, it is worth noticing that calculations here reported suggests that the increasing of the resonance is not related to the oxidation of the gold clusters but rather it corroborates a depleting of the metallic band

which, eventually indicates a partial positive charging of the clusters.

In comprehensive studies, it has already been reported that ionic gold is not participating in the oxidation of CO [16, 26]. In addition, it was also suggested that the small gold clusters are the only active species, so the catalytic activity is related to bridged surface groups adsorbed on interfacial Au atoms of these small particles which, for instance, in the case of water shift gas reaction are the OH groups [16]. In constrast with the reported results, [14,16,26] which were obtained with low resolution XAS, our findings prove the existence of partially charged metal clusters originated by the temporary empyting of the gold d band during the oxidation reaction.

Moreover, the results support the possible mechanism of CO oxidation over Au/CeO_2 catalyst in which molecular oxygen adsorbs onto defect sites at the gold–ceria interface and are consumed by reaction with adsorbed CO. In this, lattice oxygen from the support is consumed by reaction with CO and replenished by molecular oxygen [49].

Conclusions

Nanosized gold catalysts supported on ceria are investigated by *in situ* HERFD-XAFS at the Au L3-edge during treatments with O2 and CO, and time-resolved measurements revealed the active role of 5d orbitals from Au metal during the CO oxidation. Experimental data evidenced that the occupancy of the 5d band is reversible when reductive or oxidizing conditions are switched. An oscillating behavior of the XANES resonance peak is evident during the O2 treatment oxygen, which can be related to the oscillating variation of the population of 5*d* band during the oxidation process. XANES spectra were also modeled ab initio, confirming that the variations in the 5d band occupancy result in variations of the core-hole screening.

References

[1] M. Haruta, T. Kobayashi, H. Sano, N. Yamada, Chem. Lett. 1987, 405.

[2] X. Liu, M.H. Liu, Y. C. Chia Luo, C.Y. Mou, S.D. Lin, H. Cheng, J.M. Chen, J.F. Lee, T.S. Lin, J. Am. Chem. Soc. 2012, 134, 10251−10258.

[3] Y. Liu, C. J. Jia, J. Yamasaki, O. Terasaki, F. Schuth, Angew. Chem., Int. Ed. 2010, 49, 5771.

[4] M. Valden, X. Lai, D. W. Goodman, Onset of catalytic activity of gold clusters on titania with the appearance of nonmetallic properties. Science 281,1647–1650 (1998).

[5] A. A. Herzing, C. J. Kiely, A. F. Carley, P. Landon, G. J. Hutchings, Identification of active gold nanoclusters on iron oxide supports for CO oxidation. Science 321, 1331–1335 (2008).

[6] S. Carrettin, P. Concepciòn, A. Corma, A., J. M. López Nieto, V. F. Puntes, Nanocrystalline CeO_2 increases the activity of Au for CO oxidation by two orders of magnitude. Angew. Chem. Int. Ed. 43, 2538–2540 (2004).

[7] R. Si, M. Flytzani-Stephanopoulos, Shape and crystal-plane effects of nanoscale ceria on the activity of Au-CeO_2 catalysts for the water–gas shift reaction. Angew. Chem. Int. Ed. 47, 2884–2887 (2008).

[8] D. Widmann, R.J. Behm, Activation of molecular oxygen and the nature of the active oxygen species for CO oxidation on oxide supported Au catalysts. Acc. Chem. Res. 47, 740–749 (2014).

[9] D. Widmann, R.J. Behm, Active oxygen on a Au/TiO_2 catalyst: formation, stability, and CO oxidation activity. Angew. Chem. Int. Ed. 50, 10241–10245 (2011).

[10] Q. Fu, H. Saltsburg, M. Flytzani-Stephanopoulos, Active nonmetallic Au and Pt species on ceria-based water-gas shift catalysts. Science 301, 935–938 (2003).

[11] López-Haro, M. et al. Imaging nanostructural modifications induced by electronic metal-support interaction effects at Au parallel to cerium-based oxide nanointerfaces. ACS Nano 6, 6812–6820 (2012).

[12] G. Kumar, L. Tibbitts, J. Newell, B. Panthi, A. Mukhopadhyay, R. M. Rioux, C. J. Pursell, M. Janik and B. D. Chandler, Evaluating differences in the active-site electronics of supported Au nanoparticle catalysts using Hammett and DFT studies, Nature Chemistry, 2018,10, 268–274.

[13] Y.-G. Wang, D. Mei, V.-A. Glezakou, J. Li, R. Rousseau, Dynamic formation of single-atom catalytic active sites on ceria-supported gold nanoparticles, Nature Comm., 2015 DOI: 10.1038/ncomms7511

[14] L.-W. Guo, P.-P. Du, X.-P. Fu, C. Ma, J. Zeng, R. Si, Y.-Y. Huang, C.-J. Jia, Y.-W. Zhang, C.-H. Yan, Contributions of distinct gold species to catalytic reactivity for carbon monoxide oxidation, Nature Comm, 2016, DOI: 10.1038/ncomms13481

[15] Y. Hea, J.-C. Liu, L. Luod, Y.-G. Wangb, J. Zhue, Y. Dug, J. Li, S.X. Maoa, C. Wang, Size-dependent dynamic structures of supported gold nanoparticles in CO oxidation reaction condition, PNAS, 2018, vol. 115, 30, 7700–7705.

[16] X.-P. Fu, L.-W. Guo, W.-W. Wang, C. Ma, C-J. Jia, K. Wu, R. Si, L.-D. Sun, C.-H. Yan, Direct Identification of Active Surface Species for the Water−Gas Shift Reaction on a Gold−Ceria Catalyst, *J. Am. Chem. Soc*. 2019, 141, 4613−4623.

[17] H. Hakkinen, S. Abbet, A. Sanchez, U. Heiz, U. Landman, Structural, Electronic, and Impurity-Doping Effects in Nanoscale Chemistry: Supported Gold Nanoclusters, Angew. Chem. Int. Ed. 2003, 42, No. 11

[18] B. Yoon, H. Hakkinen, U. Landman, A. S. Worz, J.-M. Antonietti, S. Abbet, K. Judai, U. Heiz, Charging Effects on Bonding and Catalyzed Oxidation of CO on Au8 Clusters on MgO, Science, 2005, 307, 21, 403-407.

[19] Why gold is the noblest of all the metals, B. Hammer & J. K. Norskov Nature volume 376, pages238–240(1995)

[20] J. A. van Bokhoven,C. Louis, J. T. Miller, M. Tromp, O. V. Safonova, Pieter Glatzel, Activation of Oxygen on Gold/Alumina Catalysts: In Situ High-

Energy-Resolution Fluorescence and Time-Resolved X-ray Spectroscopy, Angew. Chem. 2006, 118, 4767 –4770

[21] P. Glatzel, J. Singh, K. O. Kvashnina, J. A. van Bokhoven, J. Am. Chem. Soc. 2010, 132, 2555–2557.

[22] N. Weiher, A. M. Beesley, N. Tsapatsaris, L. Delannoy, C. Louis, J. A. van Bokhoven, S. L. M. Schroeder, Activation of Oxygen by Metallic Gold in Au/TiO2 Catalysts, J. AM. CHEM. SOC. 2007, 129, 2240-2241

[23] A. Visikovskiy, H. Matsumoto, K. Mitsuhara, T. Nakada, T. Akita, Y. Kido, (2011). "Electronic d-band properties of gold nanoclusters grown on amorphous carbon". Physical Review B. 83 (16): 165428

[24] C. Tian, H. Zhang, X. Zhu, B. Lin, X.i Liu, H. Chen, Y. Zhang, D. R. Mullins, C. W. Abney, M. Shakouri, R. Chernikov, Y. Hu, F. Polo-Garzon, Z. Wu, V. Fung, D. Jiang, X. Liu, M. Chi, J. Liu, S. Dai, A new trick for an old support: Stabilizing gold single atoms on $LaFeO_3$ perovskite, App. Catal. B: Environmental, 2020, 261, 118178.

[25] A. Corma, P. Concepción, M. Boronat, M. J. Sabater, J. Navas, M. J. Yacaman, E. Larios, A. Posadas, M. A. López-Quintela, D. Buceta, E. Mendoza, G. Guilera and A. Mayoral, Exceptional oxidation activity with size-controlled supported gold clusters of low atomicity, Nature Chemistry, 2013, 5, 775, 781.

[26] A. M. Abdel-Mageed, G. Kučerová, J. Bansmann, and R. J. Behm, Active Au Species During the Low-Temperature Water Gas Shift Reaction on Au/CeO2: A Time-Resolved Operando XAS and DRIFTS Study, ACS Catal. 2017, 7, 6471−6484.

[27] G. Pacchioni, Phys. Chem. Chem Phys. 2013, 15, 1737-1757.

[28] J. T. Miller, A. J. Kropf, Y. Zha, J.R. Regalbuto, L. Delannoy, C. Louis, E. Bus, J.A. van Bokhoven, J. Catal. 2006, 240, 222

[29] A. Longo, L.F. Liotta, G. Pantaleo, F. Giannici, A.M. Venezia, A. Martorana, J. Phys. Chem. C 2012, 116, 2960−2966.

[30] J. Singh, M. Tromp, O. V. Safonova, P. Glatzel, J. A. van Bokhoven, Catalysis Today 145 (2009) 300–306
[31] A. S. Hoffman, D. Sokaras S. Zhang, L. M. Debefve, C-Yu Fang, A. Gallo, T. Kroll, D. A. Dixon, S. R. Bare, B. C. Gates, Chemistry a European Journal 23 (2017)14760-14768
[32] O. Bunau and Y. Joly “Self-consistent aspects of x-ray absorption calculations“ J. Phys.: Condens. Matter 21, 345501 (2009).
[33] M.P. Casaletto, A. Longo, A.M. Venezia, A. Martorana, A. Prestianni, Metal-support and preparation influence on the structural and electronic properties of gold catalysts, Applied Catalysis A: General 302 (2006) 309–316.
[34] A.M. Venezia, G. Pantaleo, A. Longo, G. Di Carlo, M.P. Casaletto, F.L. Liotta, G. Deganello, Relationship between Structure and CO Oxidation Activity of Ceria-Supported Gold Catalysts, *J. Phys. Chem. B* 2005, *109,* 2821-2827
[35] P.M.A. Sherwood, D. Briggs, M.P. Seah (Eds.), Data Analysis in X-ray Photoelectron Spectroscopy in Practical Surface Analysis by Auger and X-ray Photoelectron Spectroscopy, Wiley, New York (1990) p. 1
[36] C.D. Wagner, L.E. Davis and W.M. Riggs, Surf. Interface Anal., 2 (1986), p. 5
[37] NIST Standard Reference Database 20, Version 3.4
[38] P. Glatzel, U. Bergmann, Coord. Chem. Rev. 2005, 249, 65.
[39] M. Moretti Sala, K. Martel, C. Henriquet, A. Al Zein, L. Simonelli, C. Sahle, H. Gonzalez, M.-C. Lagier, C. Ponchut, S. Huotari, R. Verbeni, M. Krisch and G. Monaco, J. Synchrotron Rad. (2018). 25, 580-591

[40] A. Filipponi, A. Di Cicco, Phys. Rev. B 1995, 52, 15135.
[41] Y. Joly, Y. X-ray absorption near-edge structure calculations beyond the muffin-tin approximation. Phys. Rev. B - Condens. Matter Mater. Phys. 2001,

63, 125120.
[42] S.A. Guda, A. A. Guda, M. A. Soldatov, K. A. Lomachenko, A. L. Bugaev, C. Lamberti, W. Gawelda, C. Bressler, G. Smolentsev, A. V. Soldatov, Y. Joly, Optimized Finite Difference Method for the Full-Potential XANES Simulations: Applicationto Molecular Adsorption Geometries in MOFs and Metal-Ligand Intersystem Crossing Transients. J. Chem. Theory Comput. 2015, 11, 4512–4521.
[43] A. Balerna, E. Bernieri, P. Picozzi, A. Reale, S. Santucci, E. Burattini, S. Mobilio, Extended x-ray-absorption fine-structure and near-edge-structure studies, on evaporated small clusters of Au, Phys. Rev. B, 1985, 31,5058-5065.
[44] A. Balerna, S. Mobilio, Dynamic properties and Debye temperatures of bulk Au and Au clusters studied using extended x-ray-absorption fine-structure spectroscopy, Phys. Rev. B, 1986,34,4,2293-2298.
[45] P. Zhang, T. K. Sham, X-Ray Studies of the Structure and Electronic Behavior of Alkanethiolate-Capped Gold Nanoparticles: The Interplay of Size and Surface Effects Phys. ReV. Lett. 2003, 90, 245502
[46] P. Zhang, T. K. Sham, Tuning the electronic behavior of Au nanoparticles with capping molecules, T. K. Appl. Phys. Lett. 2002, 81, 736.
[47] M.P. Casaletto, A. Longo, A. Martorana, A. Prestianni, A. M. Venezia, XPS study of supported gold catalysts: the role of Au^0 and $Au^{+\delta}$ species as active sites, Surf and Interface Anal, 2006,38, 215,218
[48] C. Schilling, C. Hess, Elucidating the Role of Support Oxygen in the Water−Gas Shift Reaction over Ceria-Supported Gold Catalysts Using Operando Spectroscopy ACS Catal. 2019, 9, 1159−1171
[49] M. Lohrenscheit, C. Hess, Direct Evidence for the Participation of Oxygen Vacancies in the Oxidation of Carbon Monoxide over Ceria-Supported Gold Catalysts by using Operando Raman Spectroscopy, ChemCatChem 2016, 8, 523 – 526.

[50] J. Guzman, S. Carrettin, J. C. Fierro-Gonzalez, Y. Hao, B. C. Gates, A. Corma, CO Oxidation Catalyzed by Supported Gold: Cooperation between Gold and Nanocrystalline Rare-Earth Supports Forms Reactive Surface Superoxide and Peroxide Species, Angew. Chem. Int. Ed. 2005, 44, 4778 – 4781

[51] Z.-K. Han, Y.-G. Wang, Y. Gao, Catalytic role of vacancy diffusion in ceria supported atomic gold catalyst, Chem. Commun., 2017, 53, 9125

[52] Y. Joly, Physical Review B 2001, 63 (12), 125120. 29.

[53] Y. Joly, Phys Rev Letter, 2002, 82, (11) 2398-2401.